JOURNAL OF GEOPHYSICAL RESEARCH, VOL. 87, NO. A7, PAGES 5267–5274, JULY 1, 1982

An Analysis of the Structure of Saturn's Magnetic Field Using Charged Particle Absorption Signatures

D. L. CHENETTE[1] AND LEVERETT DAVIS, JR.

California Institute of Technology, Pasadena, California 91125

A new technique is derived for determining the structure of Saturn's magnetic field. This technique uses the observed positions of charged particle absorption signatures due to the satellites and rings of Saturn to determine the parameters of an axially symmetric, spherical harmonic model of the magnetic field using the method of least squares. Absorption signatures observed along the Pioneer 11, Voyager 1, and Voyager 2 spacecraft trajectories are used to derive values for the orientation of the magnetic symmetry axis relative to Saturn's axis of rotation, the axial displacement of the center of the magnetic dipole from the center of Saturn, and the magnitude of the external field component. Comparing these results with the magnetic field model parameters deduced from analyses of magnetometer data leads us to prefer models that incorporate a northward offset of the dipole center by about 0.05 R_s.

1. INTRODUCTION

The nearly dipolar nature of Saturn's magnetic field and its near symmetry about Saturn's axis of rotation are among the remarkable discoveries that have resulted from the recent encounters of the Pioneer 11, Voyager 1, and Voyager 2 spacecraft with Saturn [*Smith et al.*, 1980*a*; *Acuña and Ness*, 1980; *Ness et al.*, 1981, 1982]. The deviations from this symmetry, however, while small, may be important for understanding other processes occurring at Saturn. For example, the kilometric radio emissions from Saturn are strongly modulated by Saturn's rotation [*Kaiser et al.*, 1981, and references therein]. This modulation appears to require a longitudinal asymmetry of Saturn's magnetic field. In addition, the effect of a tilt and an offset of the internal magnetic field dipole has been considered in models of the Saturnian electrostatic discharges and the spokes in Saturn's rings [*Goertz et al.*, 1981]. Reliable estimates of the nonaxial and higher order moments of the Saturnian magnetic field are necessary to characterize accurately the field and thus to understand better the structure of Saturn's magnetosphere and the mechanisms responsible for these rotationally-modulated phenomena.

Spherical harmonic analyses of the measured magnetic field at Saturn have been performed by using data from the Pioneer 11, Voyager 1, and Voyager 2 magnetometers. While these analyses have yielded consistent values for the magnitude of the magnetic dipole moment, estimates of some of the higher order terms resulting from these fits have varied. The analysis of Pioneer 11 vector helium magnetometer data presented by *Smith et al.* [1980*b*] yielded a dipole that was offset by ~0.05 R_s north of the center of Saturn and implied a dipole tilt of ~1° but with an ill-defined tilt direction, generally in the quadrant 270°–360° Saturn longitude system (SLS; see *Desch and Kaiser* [1981] for the definition of SLS). In addition, the results of the Pioneer 11 flux gate magnetometer data analysis presented by *Acuña et al.* [1980] were consistent with a 0.04 R_s north polar offset. The analysis of Voyager 1 data presented by *Acuña et al.* [1981] yielded a tilt of ~1°, toward an SLS longitude of ~340°, in agreement with the Pioneer 11 results. However, these Voyager 1 data gave a negligible (<0.02 R_s) dipole offset. The most recent, but preliminary, analysis using Voyager 2 magnetic field magnitude data combined with Voyager 1 vector data also yielded a centered dipole, but tilted by 0.8° towards 284° SLS [*Ness et al.*, 1982]. Each of these studies suffers from the restricted spatial coverage of the individual spacecraft trajectories (Figure 1), with the result that some of the parameters of the models are poorly determined. Better models of Saturn's field will undoubtedly result when data from these different spacecraft are combined. At the present time, however, there is a significant disagreement between the various Pioneer 11, Voyager 1, and Voyager 2 models on the magnitude of any polar offset of Saturn's magnetic field dipole. It is this disagreement that has motivated the study presented here.

In this paper we derive a new method for determining the geometry of Saturn's magnetic field that is independent of direct measurements of the field. This method is related to the earlier methods originated by *Van Allen et al.* [1974] and used by *Simpson et al.* [1980] and *Vogt et al.* [1982] that used energetic particle data to discriminate between a finite number of specific dipole models of the magnetic field or used a graphical procedure to interpolate between them. In these methods, L values were computed along the inbound and outbound trajectories of the spacecraft for each model and the particle fluxes were plotted against this L. The choice of models was based on the degree of similarity or difference between the inbound and the outbound data much as in Figure 2 below. Our new method describes the magnetic field model numerically in terms of parameters such as the Gaussian coefficients of an axially symmetric model or as the position and tilt of a dipole. We obtain a quantitative measure of the goodness of fit of the model as a function of these parameters, and we minimize this measure by the usual least-squares procedure to get the 'best' values for the parameters that define the model.

The many satellites and rings surrounding Saturn provide a set of test probes of the magnetosphere by absorbing energetic charged particles (Figure 2). Since charged particles closely follow magnetic field lines in the course of their latitudinal bounce motion, the signatures that result from

[1]Also at Space Sciences Laboratory, The Aerospace Corporation, Los Angeles, California 90009.

Paper number 2A0577.
0148-0227/82/002A-0577$05.00

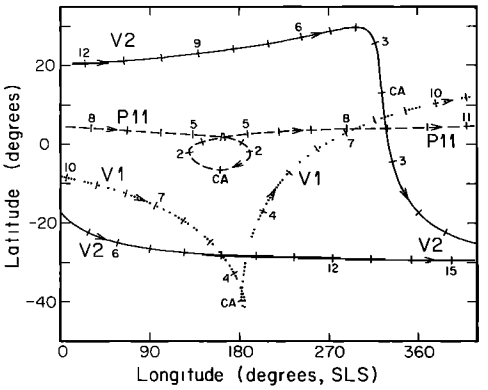

Fig. 1. The sub-spacecraft latitude and longitude traces of Pioneer 11 (dashed line), Voyager 1 (dotted line), and Voyager 2 (solid line), in Saturnographic coordinates. Numbered tic marks along these traces indicate the radial distance of each spacecraft from Saturn in Saturn radii. The position of each spacecraft at its closest approach to Saturn is shown by the tic labeled 'CA.'

satellite and ring absorption can be used to trace the shapes of field lines in latitude. In addition, since the energetic charged particles drift in longitude on L shells that enclose a constant magnetic flux, these signatures also provide a measure of the azimuthal field geometry. With the new method that is presented in this report it is possible to calculate the coefficients of the axially symmetric, spherical harmonic magnetic field model that give the best approximation to the shape of Saturn's magnetic field as determined from the positions of these charged particle absorption features. In this method the axis of symmetry need not coincide with the rotation axis; the coefficients of the expansion and the parameters that define the axis of symmetry can be simultaneously determined by a least squares fit using the positions where charged particle absorption signatures were observed.

Figure 2 illustrates how absorption signatures can be used to deduce the field geometry. If Saturn's magnetic field were that of a dipole, then the quantity $L = r_d/\cos^2\lambda_d$, where r_d is the distance of the spacecraft from the center of the dipole and λ_d is its latitude from the dipole equator, should organize the positions of these absorption signatures. The signatures should appear at the same L both inbound and outbound and that L should be L_M the L shell coordinate of the object which produced the signature. (In a later section of this paper we show that the effects of L shell eccentricity and splitting on these data are small enough to be ignorable.) In Figure 2*a* the dipole was assumed to be centered on Saturn and aligned with Saturn's rotation axis. Using the 63- to 160-MeV proton counting rate measured by the cosmic ray system on Voyager 2 [*Vogt et al.*, 1982] for this assumed field geometry, absorption signatures of Mimas and Enceladus appear at $L > L_M$ inbound when the spacecraft was in the northern hemisphere ($\lambda \sim 20°$), and at $L < L_M$ outbound in the southern hemisphere ($\lambda \sim -10°$). Thus the data of Figure 2*a* provide evidence for a deviation of the field from this simplest model, a deviation that is antisymmetric between the northern and southern hemispheres along the Voyager 2 trajectory.

Two alternative models may be invoked to organize better the data of Figure 2*a*: a northward offset of the dipole center (equivalent to a small, positive quadrupole moment), or, since these data cover a restricted range of Saturn longitudes (Figure 1), a tilt of the dipole away from the longitude of the spacecraft. The effect of incorporating a 0.05 R_s offset of the dipole center is illustrated in Figure 2*b*. Alternatively, tilting the dipole by 1.7° toward 180° SLS provides an equivalent improvement in organizing these data. The basic ambiguity between a tilt and an offset can be resolved by incorporating more data that cover a larger longitude range. Thus in the analysis presented here we have combined absorption signature observations from the Pioneer 11, Voyager 1, and Voyager 2 spacecraft (whose trajectories are shown in Figure 1) to determine the parameters of the axially symmetric magnetic field model which provide the best description of these energetic charged particle data. The results of this analysis will be compared with the models based on analyses of the magnetometer data to discriminate among the various models for Saturn's magnetic field.

Analyses of Saturn's magnetic field geometry based on charged particle data, but using a graphical technique rather than the least squares method presented here, have been published. *Simpson et al.* [1980] have used charged particle data from Pioneer 11 to constrain the possible equatorial offset of the dipole. *Vogt et al.* [1982] have presented a study of the possible tilt and north-south offset of Saturn's dipole using absorption signatures observed on Voyager 2.

2. Method of Analysis

If we assume that Saturn's magnetic field is adequately represented by an axially symmetric model, we can estimate some of the low-order parameters of this model from the positions of points on the L shells where the flux of energetic charged particles is decreased through absorption by Saturn's satellites. To do this requires that we know the positions of at least two points on each of several such shells. These two points may be determined from two positions of a spacecraft as it crosses a given shell inbound and outbound, or from the position of the absorber that produced the observed signature and one spacecraft position. Since the time between the formation of these signatures and their observation at the spacecraft is short, ranging from less than a minute to a maximum of ~23 hours at Mimas (the orbital period of Mimas), we neglect the effect of radial diffusion on the positions of the signatures.

We assume that the axially symmetric field is defined in the usual way by the coefficients (g_n^0, G_n^0) in the spherical harmonic representation of the scalar potential:

$$\Phi(r, \theta, \varphi) = a\left[g_1^0\left(\frac{a}{r}\right)^2 P_1(\cos\theta) + g_2^0\left(\frac{a}{r}\right)^3 P_2(\cos\theta) + \cdots + G_1^0\left(\frac{r}{a}\right) P_1(\cos\theta) + G_3^0\left(\frac{r}{a}\right)^3 P_3(\cos\theta) + G_5^0\left(\frac{r}{a}\right)^5 P_5(\cos\theta) + \cdots\right] \quad (1)$$

where r is radial distance from Saturn, a is the nominal equatorial radius of Saturn, and the P_n are Legendre functions. The magnetic field is

$$\mathbf{B}(r, \theta, \varphi) = -\nabla\Phi \quad (2)$$

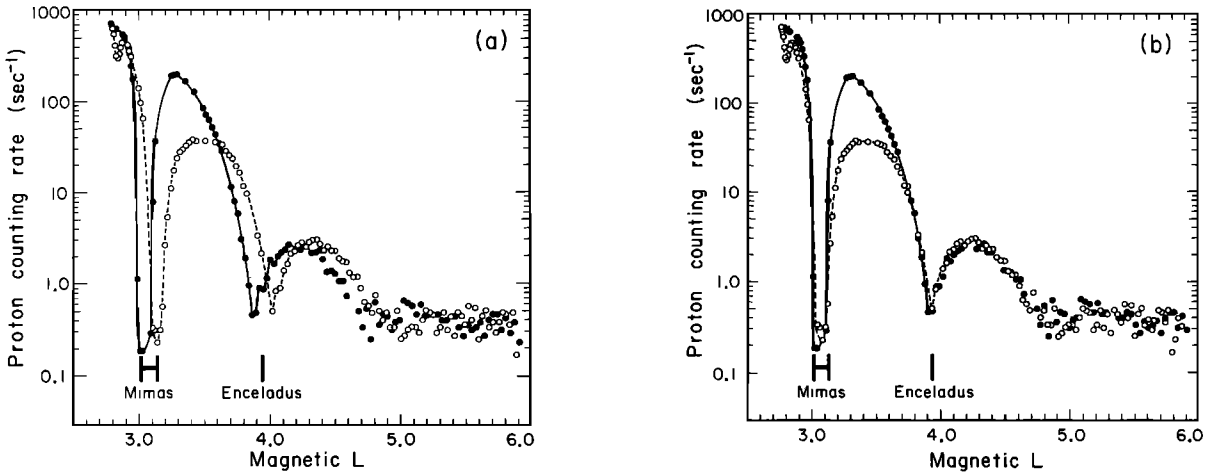

Fig. 2. The counting rate from the cosmic ray system on Voyager 2, which responds to protons in the energy range 63- to 160-MeV, plotted versus L, for two different dipole magnetic field models. In part (*a*), the dipole was assumed to be centered on Saturn, while in part (*b*) the dipole was assumed to be offset north by 0.05 Saturn radii. In both cases the dipole was assumed to be aligned with Saturn's axis of rotation. Open symbols connected by dashed lines represent data obtained along the inbound pass. Filled symbols connected by solid lines represent data from the outbound pass. The positions of two of Saturn's inner satellites are indicated.

More terms could be included in (1) if desired, but because of the limited data available we consider only cases involving these low-order terms. Additionally, the higher order external field terms G_3^0 and G_5^0 can be constrained by requiring that the ratios G_3^0/G_1^0 and G_5^0/G_1^0 have the values that would be produced, for example, by the ring current model of *Connerney et al.* [1981]. Thus it may be possible to test whether or not this ring current field is preferable to a uniform field as a model for the effect on the charged particle signatures of the external component of the field in the inner magnetosphere.

The magnetic field need not be axially symmetric in a system based on the rotation axis of Saturn. The symmetry is necessary only in a coordinate system based on the magnetic axis. Given an assumed tilt angle (α) and longitude (δ) of the magnetic axis in Saturnographic coordinates, the coordinates of any positions are easily converted from the Saturnographic coordinate system to this magnetic coordinate system. Estimates of the tilt angle and its longitude in the Saturnographic system may be made by finding the values of α and δ which give the best fit of the model to the charged particle observations.

If the magnetic field has the axial symmetry in the magnetic coordinate system defined by (1) and (2), the L shells are surfaces of revolution characterized by the magnetic flux through them. Define the flux function:

$$\Psi(r, \theta) = \int_0^v B_r r^2 \sin\theta d\theta \tag{3}$$

Each L shell is uniquely identified by the value of this function. For the field defined by (1), taking $a = 1\ R_s$ = 60330 km, the nominal equatorial radius of Saturn, and using, as coordinates, r (in units of R_s) and λ (the latitude relative to the magnetic equator), the flux function is given by

$$\frac{\Psi(r, \lambda)}{g_1^0 R_s^2} = \left[\frac{\cos^2\lambda}{r} + Z\frac{3\cos^2\lambda\sin\lambda}{r^2} - U_1\frac{1}{2}r^2\cos^2\lambda + U_3\frac{3}{8}r^4\cos^2\lambda(1 - 5\sin^2\lambda) - U_5 r^6\cos^2\lambda \cdot (1 - 14\sin^2\lambda + 21\sin^4\lambda)\right] \tag{4}$$

where $Z = g_2^0/(2g_1^0)$ and $U_n = G_n^0/g_1^0$. It is convenient to express Ψ in this form since only the ratios Z and U_n, not the Gaussian coefficients g_n^0 and G_n^0, can be determined from the energetic charged particle absorption signatures. The positions of the signatures are sensitive only to the shape of the field and thus are independent of an overall scale factor that determines the magnitude of the field. If Z is small (<0.1), the value of Z may be interpreted as the displacement of the center of an equivalent dipole from the center of Saturn (in units of R_s), either north ($Z > 0$) or south ($Z < 0$) along the magnetic symmetry axis [*Smith et al.*, 1976; *Acuña et al.*, 1980].

To determine the parameters of this model, the functions of r and λ on the right-hand side of (4) are evaluated at pairs of points on each L shell identified by particle signatures. Then D_i, the difference between $\Psi(r, \lambda)/(g_1^0 R_s^2)$ for the ith pair of points on the same L shell is a linear function of the coefficients Z and U_n. The desired estimates of these coefficients can be found by minimizing

$$R^2(Z, U_n, \alpha, \delta) = \sum_{i=1}^{m} D_i^2 \tag{5}$$

using a least squares method. If we wish to determine the longitude δ and tilt angle α of the magnetic axis of symmetry relative to Saturn's rotation axis, the problem becomes nonlinear and a numerical procedure is required. The numerical method that we have used to minimize R^2 is based on the procedure described by *Powell* [1964]. The standard deviations of the parameters presented in this report are the formal statistical errors calculated from the curvature matrix of the function at the minimum [*Bevington*, 1969]. In the following sections of this paper we refer to the root mean square residual of the fit, which we define as RMS = $(R^2/m)^{1/2}$, and the 'goodness of fit,' which we define as $[R^2/(m-n)]^{1/2}$, where m is the number of D_i terms in R^2, and n is the number of coefficients varied in the fit. Better fits to the data are indicated by smaller values of this 'goodness of fit' parameter.

TABLE 1. Absorption Signature and Satellite Coordinate Pairs

Object*	R, R_s	Latitude, deg.	Longitude, deg., SLS	Object*	R, R_s	Latitude, deg.	Longitude, deg., SLS	Data Sets
V2, I	2.727	19.19	321.63	Mimas, P	3.014	...	...	A, B, C
V2, O	2.989	−3.94	334.35	Mimas, P	3.014	...	...	A, B, C
V2, I	2.776	21.23	320.71	Mimas, A	3.140	...	...	A, B, C
V2, O	3.093	−6.26	336.92	Mimas, A	3.140	...	...	A, B, C
V2, I	3.162	27.38	314.82	Enceladus	3.950	...	...	A, B, C
V2, O	3.670	−14.40	351.30	Enceladus	3.950	...	...	A, B, C
V2, O	4.283	−19.09	7.62	Tethys	4.885	−0.95	6.48	A, B, C
V1, O	8.377	7.03	330.09	Rhea	8.729	−0.33	331.74	B, C
P11, I	3.167	0.40	179.30	P11, O	3.173	0.72	142.93	C
P11, I	3.044	0.19	181.52	P11, O	3.063	0.53	140.93	C
P11, I	2.669	−0.58	187.22	P11, O	2.679	−0.24	135.03	C
P11, I	2.550	−0.87	188.62	P11, O	2.558	−0.54	133.57	C
P11, I	2.363	−1.38	190.33	P11, O	2.366	−1.07	131.81	C
P11, I	2.345	−1.44	190.45	P11, O	2.347	−1.12	131.67	C
P11, I	2.328	−1.49	190.56	P11, O	2.329	−1.18	131.56	C

*V2: Voyager 2; V1: Voyager 1; P11: Pioneer 11; I: inbound; O: outbound; P: Mimas periapsis radius; A: Mimas apoapsis radius.

Connerney et al. [1981] have proposed that the external source coefficients, the G_n^0, are predominantly determined by a ring current. The current density in the model they prefer is, using cylindrical coordinates (ρ, θ, z):

$$J(\rho, \theta, z) = \begin{cases} J_0 R_s/\rho & \text{if } \rho_1 \le \rho < \rho_2 \text{ and } |z| \le z_0 \\ 0 & \text{otherwise} \end{cases} \quad (6)$$

where $J_0 = 2.4 \times 10^6\ A/R_s^2$, $z_0 = 2.5\ R_s$, $\rho_1 = 8.5\ R_s$, and $\rho_2 = 15.5\ R_s$. The magnetic field produced in the region where r is less than ρ_1 may be calculated by integrating the effect of a circular current [*Smythe*, 1968] over the volume occupied by the current. The expression of this result in terms of spherical harmonics gives

$$G_1^0 = -\frac{2\pi}{5R_s} J_0 \ln\left\{\frac{\rho_2}{\rho_1}\left[\frac{z_0 + (\rho_1^2 + z_0^2)^{1/2}}{z_0 + (\rho_2^2 + z_0^2)^{1/2}}\right]\right\} \quad (7a)$$

$$G_3^0 = -\frac{\pi R_s}{15} J_0 \left[\frac{z_0}{(z_0^2 + \rho_2^2)^{3/2}} - \frac{z_0}{(z_0^2 + \rho_1^2)^{3/2}}\right] \quad (7b)$$

$$G_5^0 = -\frac{\pi R_s^3}{100} J_0 z_0 \left[\frac{(3\rho_2^2 - 2z_0^2)}{(\rho_2^2 + z_0^2)^{7/2}} - \frac{(3\rho_1^2 - 2z_0^2)}{(\rho_1^2 + z_0^2)^{7/2}}\right] \quad (7c)$$

where J_0 is in units of A/R_s^2. If the parameters proposed by *Connerney et al.* [1981] are used, the results are $G_1^0 = -6.47$ nT, $G_3^0 = 0.0246$ nT, and $G_5^0 = -1.39 \times 10^{-4}$ nT. If we require that $U_3 = (G_3^0/G_1^0)\ U_1$ and that $U_5 = (G_5^0/G_1^0)\ U_1$ in (4) and if we also require that these ratios be consistent with the model of *Connerney et al.* [1981], leaving only J_0 as an adjustable parameter, then $U_3 = -3.80 \times 10^{-3}\ U_1$ and $U_5 = 2.16 \times 10^{-5}\ U_1$. These coefficients are small, and from (4) and the coordinates in Table 1 it is clear that the U_3 and U_5 terms are negligible for our data set, except for the Voyager 1 absorption signature at Rhea (8.8 R_s). We have tested whether this model better fits the observations in the inner magnetosphere than does the model with $U_3 = U_5 = 0.0$, which assumes that the external source produces only a uniform magnetic field. We find no significant difference in either the 'goodness of fit' (<3% change with and without these higher order terms) or in the values of the resulting best fit parameters. Thus with the present data we cannot distinguish between these models for the external field. Therefore, in the present study the external field terms are incorporated into a single parameter $U \equiv U_1$.

3. Data Sets Used in This Study

The pairs of coordinates of energetic charged particle features that were used to calculate the D_i's in this study are listed in Table 1. These data are divided into three data sets, each of which contains features from a different combination of the three spacecraft. Data set A includes only the seven coordinate pairs for features observed along the Voyager 2 trajectory. Data set B includes data set A with the addition of the Voyager 1 coordinate pair at Rhea (8 pairs). Data set C includes all 15 of the coordinate pairs available from Voyager 2, Voyager 1, and Pioneer 11.

The data of Table 1 are also divisible into three classes, each of which corresponds to a different way of using these positions. One class comprises the first six pairs of Table 1. These pairs are based on the position of Voyager 2, either inbound or outbound, when a given absorption feature was observed, and a radial position of the corresponding satellite in the Saturnographic equatorial plane. The Voyager 2 positions for these entries in Table 1 were determined from times of features in the 63- to 160-MeV proton flux measured by the cosmic ray system [*Vogt et al.*, 1982]. Absorption signatures observed in the MeV electron flux near Mimas and Enceladus on Voyager 2 are not included in this study due to problems associated with the interpretation of these signatures [*Vogt et al.*, 1982].

The features associated with Mimas and Enceladus in this first class are stable shells that are depleted of high energy protons at all longitudes because these satellites sweep out particles faster than they are replenished by radial diffusion or other means. Since these features are not dependent on the actual position of the satellite at any instant, it is appropriate to use an average position of the satellite. The depleted shell for Mimas is thick because of Mimas's large orbital eccentricity. Thus two L shells are used for the position of Mimas in this analysis. The equatorial radii of these shells were chosen as the peri- and apo-apsidal radii of Mimas. Since the orbit of Enceladus is nearly circular, a single L shell at the center of the proton flux minimum is used. The equatorial radius of this shell was chosen to be the mean orbital radius of Enceladus. Since the latitudes and

longitudes of the satellites are ignored in this class, we have, in effect, placed the satellites along the line of nodes between the magnetic equator and the Saturnographic equator for the purposes of calculating their positions in the magnetic coordinate system.

Another class of coordinate pairs in Table 1 consists of the Voyager 2 point with Tethys and the Voyager 1 point with Rhea. Since absorption signatures like these are rapidly dispersed and refilled, they were observable only because the spacecraft passed close to the longitude of the satellite as the spacecraft crossed the satellite's L shell. Thus, in this class it is appropriate to use the actual coordinates of the satellite at the estimated time when the absorption signature was formed. These signatures are discussed in more detail by *Vogt et al.* [1981, 1982].

The last class of coordinate pairs in Table 1 comprises the Pioneer 11 absorption features. These data were obtained from the University of Chicago charged particle investigation (R. B. McKibben, personal communication, 1981) and are the same features that were used in the analysis of the offset in the equatorial plane of Saturn's magnetic dipole reported by *Simpson et al.* [1980]. In this class the coordinate pairs are the positions of the spacecraft as Pioneer 11 crossed features that were identifiable on both the inbound and the outbound passes.

In the analysis presented here we have neglected any possible equatorial offset of the dipole, based on the results presented by *Simpson et al.* [1980], who concluded that the equatorial offset was less than 0.01 R_s and perhaps less than 0.003 R_s, given the interpretation of *Simpson et al.* [1980] of features associated with the absorption signature of the F ring. These results were derived before the Voyager 1 discovery that the F ring was structured and eccentric. The ±200-km variation in the distance of the F ring from Saturn [*Smith et al.*, 1981] may affect the 0.003 R_s limit on the equatorial offset of the dipole; however, the 0.01 R_s limit, which was obtained from the radial extent of all of the features in the F ring absorption region, remains an upper limit that may be reduced if the F ring eccentricity is included. Thus the neglect of any equatorial offset in our model yields a lower limit on the uncertainty in the radial position of each feature of at least 0.003 R_s, but less than 0.01 R_s.

Other effects, not included in our model, which could influence the results of this analysis include those due to axially asymmetric contributions to the magnetic field. Probably the most important of these asymmetric terms is that due to the day-night asymmetry of the magnetosphere that is produced by the solar wind. This asymmetry induces a variation with local time in the radial position of a particle drift L shell. The largest variation is expected to occur for equatorially mirroring particles, which drift along a path of constant magnetic field intensity. Thus we consider equatorial particles in our estimate of this effect. Following *Mead* [1964] and *Luhmann and Schulz* [1979], we assume a simple three-parameter asymmetric field model. In this model the field intensity at the magnetic equator is given by

$$B = \left(\frac{a}{r}\right)^3 g_1^0 + G_1^0 + \sqrt{3}\left(\frac{r}{a}\right) G_2^1 \cos\varphi \qquad (8)$$

where φ is the longitude angle measured from local midnight, and G_2^1 is the spherical harmonic coefficient responsible for the asymmetry which we consider here. Given this form for the magnetic field, equatorially mirroring particles will follow paths that deviate from circles of constant r by

$$\Delta \approx \frac{r}{\sqrt{3}}\left(\frac{r}{a}\right)^4\left(\frac{G_2^1}{g_1^0}\right)\cos\varphi \qquad (9)$$

At other latitudes, for particles with different pitch angles, drift shells should deviate from circles of constant r by less than this amount.

An estimate of G_2^1/g_1^0 for Saturn is obtained by scaling from the earth's magnetosphere. If different choices of the radius scaling factor a are made in (1) and (8), different values of the coefficients g_n^0 and G_n^0 must be used for any specific magnetic field. Applying (8) and (9) to Saturn and the earth, we assume that the shapes of these drift shells scale as the distance from the center of the planet to the subsolar point on the magnetopause, independent of the radius of the planet or its distance from the sun. Thus in going from the earth to Saturn, we will correctly scale G_2^1/g_1^0 if in both cases we take a to be one tenth of the distance to the magnetopause and keep G_2^1/g_1^0 the same. Thus, a = 1 earth radius for the earth and $a = 2\ R_s$ for Saturn. In equation (9) we use, for Saturn, the ratio $G_2^1/g_1^0 = -1.66 \times 10^{-5}/0.31 = -5.4 \times 10^{-5}$ that *Luhmann and Schulz* [1979] obtained for earth, but there is an additional factor of 2^{-4} that comes from using $a = 2\ R_s$. Hence

$$\Delta = -1.9 \times 10^{-6} r^5 \cos\varphi \qquad (10)$$

where Δ and r are measured in Saturn radii. Thus within 4 R_s we estimate that Δ is less than 0.002 R_s, which is less than the typical radial uncertainty Δr of the features in this region ($\Delta r > 0.003\ R_s$ up to a maximum of $\Delta r \sim 0.02\ R_s$ at Enceladus). At Tethys where $\Delta r \sim 0.004\ R_s$, and Rhea where $\Delta r \sim 0.03\ R_s$, the effect of the asymmetric term is still small compared to Δr because of the small longitude difference (~1°) between the satellite and the spacecraft.

4. Results

The best fit spherical harmonic coefficients which resulted from minimizing R^2 are summarized in Table 2 and Figure 3. In this study, a different combination of the parameters of R^2 was fitted in each of four cases. The parameters that were fitted in each case are those for which there are nonzero entries in Table 2. In each run, parameters that were not varied were deleted from the fit by fixing their values to be zero. In case 1 all four parameters were varied to obtain the best fit: the dipole offset (Z), the external field term (U), and the tilt angle (α) and direction (δ). In case 2 only the offset and external field terms were varied (2 parameters), in case 3 only the external field term and the tilt were varied (3 parameters), and in case 4 only the tilt was varied (2 parameters) to obtain the best fit.

To guarantee the stability of the results that were obtained from these fits, and to judge their sensitivity to uncertainties in the coordinates of Table 1, two kinds of selection criteria were applied. Only those results that passed both criteria are presented. The first criterion was that consistent results must be obtained from each fit when individual coordinate pairs were deleted from the data set. This requirement helped to insure that no single observation dominated the result. The second criterion applied was that consistent values must be obtained from each fit when individual

TABLE 2. Results of Least Squares Fits

Case	Data Set	m, n*	Z, R_s	$U, 10^{-4}$	α, deg.	δ, deg., SLS	RMS, 10^{-4}
1	C	15, 4	0.06 ± 0.03	−7.0 ± 1.7	0.85 ± 0.58	25. ± 47.	23.4
2	A	7, 2	0.046 ± 0.002	−3.5 ± 0.8	0	...	13.9
2	B	8, 2	0.048 ± 0.004	−5.1 ± 1.2	0	...	24.4
2	C	15, 2	0.048 ± 0.004	−5.2 ± 1.4	0	...	29.5
3	A	7, 3	0	−14. ± 4.	3.2 ± 0.8	85. ± 8.	10.8
3	B	8, 3	0	−11. ± 1.	2.4 ± 0.3	92. ± 4.	11.2
3	C	15, 3	0	−10. ± 3.	2.4 ± 0.7	92. ± 10.	31.1
4	A	7, 2	0	0	1.4 ± 0.2	178. ± 13.	23.0
4	B	8, 2	0	0	1.3 ± 0.5	177. ± 28.	50.3
4	C	15, 2	0	0	1.4 ± 0.4	182. ± 21.	45.1

*m: number of coordinate pairs in fit; n: number of free parameters in fit.

coordinates were varied by the estimated uncertainty in the position of each feature. Through this method we could judge the sensitivity of the results to uncertainties in the coordinates and could ensure that we were not 'fitting the noise.' Owing to the narrow range of longitudes spanned by the Voyager 2 and Voyager 1 features, the results obtained from data sets A and B in case 1 (all four parameters free to vary) did not pass these selection criteria, and thus they have been excluded. Similarly, owing to the near-equatorial trajectory of Pioneer 11 near Saturn and the narrow range of latitudes and longitudes spanned by the Pioneer 11 data of Table 1, fits using only Pioneer 11 data did not pass these selection criteria. Otherwise, in all other cases, the calculated best fit parameters remained consistent, given the calculated standard deviations of the parameters.

From the agreement between the parameter values calculated for the three sets of features in each of cases 2, 3, and 4, we conclude that the Voyager and Pioneer 11 data are consistent with each other in the sense that the same field model can provide an equivalent organization of the various features observed on each spacecraft. The notable exception to this conclusion is indicated by the large value for the 'goodness of fit' (Figure 3) obtained in case 4, when the Voyager 1 absorption signature at Rhea is included. The explanation for this poor fit is that the dominant component affecting the deviation in the position of the Rhea absorption signature from the position expected from a pure dipole field model is the external source term, as demonstrated by *Connerney et al.* [1981] and *Vogt et al.* [1981]. The Rhea signature is poorly fit in case 4 because in this case the external field component was ignored ($U = 0$). Nevertheless, in each case the 'best-fit' parameter values remained the same whether or not the Rhea signature was included. Since consistent results are obtained from these fits by using data from all three spacecraft encounters with Saturn over a two year period, we believe that these results measure a stable state of Saturn's magnetosphere and are not dominated by short-term variations that may be induced, for example, by fluctuations in the external conditions imposed by the solar wind.

A comparison of the minimum value of R^2 tabulated as the RMS residual of each fit in Table 2, and as the 'goodness of fit' in Figure 3, provides insight to the importance of each of the parameters. For example, when case 4 is compared with any other case it is clear that the uniform external field term makes an important contribution. When it was used in the fit, the residual was significantly reduced, and the value obtained for U was different from zero by ≥3 standard deviations. In addition, comparing cases 2 and 4, which have the same number of fitted parameters, it is clear that a model incorporating a dipole offset and an external field term provides a better fit to these data than does a tilted dipole model with no external field. For cases 2 and 3, considering only the 'goodness of fit' (Figure 3) of these models to the energetic charged particle features, the fits are essentially equally good for data sets A and C, while for data set B, case 3 provides a better fit.

5. Comparison With Magnetometer-Based Field Models

To better understand the significance of the results of the previous section and to aid in discriminating among the various cases that have been explored, the axially symmetric

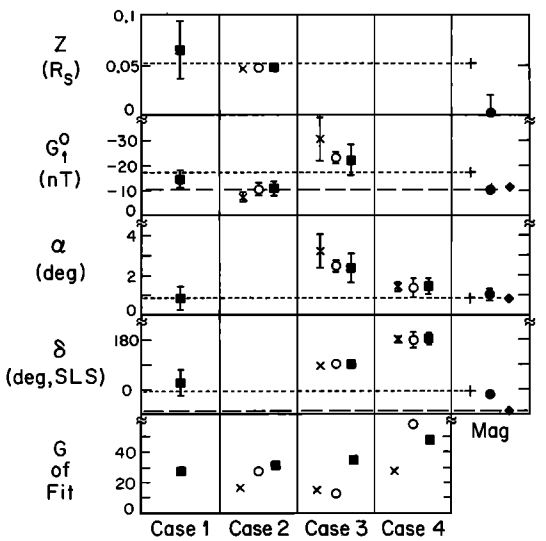

Fig. 3. A graphical representation of the best-fit parameters given in Table 2. The four different cases represent the results obtained when different combinations of the parameters were varied in the fits. Parameters that are not plotted in cases 2, 3, and 4, were fixed at zero. The solid square in each case corresponds to data set C; the open circle corresponds to data set B; and the cross corresponds to data set A, as defined in Table 1. The far-right section, labeled 'Mag' summarizes the results of Pioneer 11 (indicated by the plus symbol), Voyager 1 (indicated by the solid circle), and combined Voyager 1 and 2 (indicated by the solid diamond) models, obtained from analyses of magnetometer data. Dashed lines extend to the left from some points to facilitate the comparison of these results. Note that $G_1^0 = g_1^0 U$ is plotted, rather than U, to compare with the results of the magnetometer studies, and, for this plot, a value of the dipole moment $g_1^0 = 0.21$ G was adopted. The bottom panel of cases 1–4 summarizes the 'goodness of fit' parameter defined in the text (arbitrary units) for each of the least squares fits. Better fits are characterized by smaller values of this parameter.

TABLE 3. Calculations of R^2 Using Magnetometer Model Parameters

Name of Model*	Magnetometer Models				RMS Residual (10^{-4})		
	Z, R_s	U, 10^{-4}	α, deg.	δ, deg., SLS	Data Set A	Data Set B	Data Set C
JGR 80	0.051	−7.75	0.82	353.	80.7	75.5	59.1
P11 B	0.04	0	0	...	29.9	49.0	43.1
V1 B	0	−3.08	1.0	340.	235.	220.	163.
V1 + 2 B	0	−5.69	0.81	284.	208.	195.	145.

*Models: JGR 80, from *Smith et al.* [1980*b*]; P11 B, from *Acuña et al.* [1980]; V1 B, from *Ness et al.* [1981]; V1 + 2 B, from *Ness et al.* [1982].

model magnetic field parameters presented here are compared with field models derived from analyses of the magnetometer measurements. Part of this comparison is summarized in Figure 3.

As discussed in the introduction, either a tilt of Saturn's dipole relative to its axis of rotation, or a northward offset of the dipole center from the center of Saturn can be used to organize the positions of the satellite absorption features that have been observed. The ambiguity between these two models is reflected in the results of the previous section. Both case 2, which neglects any tilt of the dipole, and case 3, which neglects the dipole offset term, provide fits to these absorption features that are equally good, as judged by the 'goodness of fit' (Figure 3). The magnitude of the tilt in case 3, however, is 2.4–3.2°, significantly larger than the ~1° tilt that has been the consistent result of models based on the Pioneer 11 and Voyager magnetometer data. Moreover, the direction of the tilt derived in case 3 (~90° SLS) is inconsistent with the tilt directions obtained from the magnetometer analyses (270°–360° SLS). Similarly, case 4, which includes a tilted dipole but no offset or external field terms, is not only a significantly poorer fit, but it also yields a best fit tilt direction that is inconsistent with all of the magnetometer models. If the consistent results of the analyses of magnetometer data are adopted as a constraint on the selection of the best field model to use in fitting these charged particle data, then we are led to prefer cases 1 and 2, which incorporate a northward offset of the dipole, over cases 3 and 4, in which the dipole is assumed to be centered on Saturn.

The magnitudes of the dipole offsets derived in case 1 and case 2 are consistent with the values derived from the analysis of the Pioneer 11 magnetometer data [*Smith et al.*, 1980*b*; *Acuña et al.*, 1980]. Thus the present analysis of charged particle absorption signatures supports the Pioneer 11 model which incorporates a northward offset of the dipole center by ~0.05 R_s. Comparing cases 1 and 2, it is apparent that incorporating the best-fit tilt of ~1° provides only a small improvement in the 'goodness of fit' to these satellite signatures. This is, in part, why the magnitude and the direction of the tilt in case 1 have such large uncertainties. An additional effect that increases the uncertainties of both the tilt and the offset terms of case 1 arises because, with all four parameters free to vary, the fit may be only marginally overdetermined, the tilt and the offset are highly correlated. Additional absorption signatures spanning a larger range of longitudes would be required to better separate the effect of a tilt from an offset in these fits when all parameters are varied simultaneously.

Finally, in comparing the results presented here with other models of Saturn's magnetic field, we have calculated the R^2 of (5) by using several sets of parameters derived from the spherical harmonic fits to magnetometer data. As summarized in Table 3, we find that the two models based on analyses of Pioneer 11 magnetometer data, which include a north offset of the dipole center, are better fits to these charged particle absorption signatures than the two Voyager models, which do not include an offset. The RMS residual of the Pioneer 11 models is ~2 to ~10 times greater than the least squares minimum RMS residual of Table 2, while the RMS of the Voyager models is ~6 to ~30 times the minimum, i.e., ~3 times larger than the Pioneer 11 RMS for each data set. Thus, through this comparison, we are again led to prefer magnetic field models which incorporate a significant northward offset of the dipole.

6. SUMMARY

We have presented a new technique for using the observed positions of charged particle absorption signatures due to the satellites and rings of Saturn to derive the low-order terms of an axially symmetric, spherical harmonic expansion model for Saturn's magnetic field. The results that are derived from this technique depend on the geometry of the magnetic field in a way that is significantly different from analyses of vector magnetic field measurements obtained by spacecraft magnetometers. The positions of the absorption signatures are independent of the overall magnitude of the field, only the shape of the field is measured. In addition, the positions of these absorption signatures incorporate a global measure of the field geometry, spanning the latitude and longitude ranges over which they are observed.

The application of this technique to absorption signatures observed on the Pioneer 11, Voyager 1, and Voyager 2 spacecraft leads us to prefer a model that incorporates a significant northward offset of the magnetic dipole from the center of Saturn. The value for the offset that we obtain agrees with the value derived from the analyses of Pioneer 11 magnetometer data [*Smith et al.*, 1980*b*; *Acuña et al.*, 1980]. To account for the positions of these absorption signatures on the basis of an alternative model of a tilted dipole at Saturn's center would require a tilt that is inconsistent in both magnitude and direction with the tilts deduced from all magnetometer analyses.

From the perspective of the results of this paper, the 0.02 R_s upper limit to any possible dipole offset that resulted from the analysis of Voyager 1 magnetometer data [*Acuña et al.*, 1981] remains a puzzle. It seems unlikely that the offset was variable over the ~1 year intervals between the Pioneer 11 and Voyager 1, and the Voyager 1 and Voyager 2 Saturn encounters, especially since the offset obtained from this study of the charged particle data is consistent with that of the Pioneer 11 magnetometer model. An alternative, and

perhaps more plausible, hypothesis is that the contribution of the offset to the total magnetic field measured on Voyager 1 may have been masked by the nonpotential sources (current systems) suggested by the high-latitude Voyager 1 data [*Acuña et al.*, 1981]. Thus it would be interesting to examine the residuals when an offset dipole model is subtracted from the Voyager 1 data. Such a study may provide better insight to the nature of any local current systems or magnetic anomalies in Saturn's inner magnetosphere.

Acknowledgments. The Voyager cosmic ray system experiment is the result of a collaboration of groups from Caltech, Goddard Space Flight Center, the University of Arizona, and the University of New Hampshire. We are grateful to R. E. Vogt, principal investigator for this experiment, for making these Voyager data available to us. We also thank A. W. Schardt of the Goddard Space Flight Center for reducing the Voyager 2 CRS high energy proton data, R. B. McKibben and J. A. Simpson of The University of Chicago for providing the positions of the Pioneer 11 absorption signatures used in this study, and the Voyager Navigation Team of the Jet Propulsion Laboratory for providing accurate positions of the satellites of Saturn. We appreciated E. C. Stone's thoughtful suggestions and comments on an early version of this paper. This work was supported by NASA under NAS7-100 and NGR 05-002-160. DLC acknowledges additional support by the Aerospace Corporation's sponsored research program.

The Editor thanks M. H. Acuña and D. Beard for their assistance in evaluating this paper.

REFERENCES

Acuña, M. H., and N. F. Ness, The magnetic field of Saturn: Pioneer 11 observations, *Science, 207,* 444, 1980.

Acuña, M. H., J. E. P. Connerney, and N. F. Ness, The magnetic field of Saturn: Further studies of Pioneer 11 observations, *J. Geophys. Res., 85,* 5675, 1980.

Acuña, M. H., J. E. P. Connerney, and N. F. Ness, Topology of Saturn's main magnetic field, *Nature, 292,* 721, 1981.

Bevington, P. R., *Data Reduction and Error Analysis for the Physical Sciences,* pp. 242–245, McGraw-Hill, New York, 1969.

Connerney, J. E. P., M. H. Acuña, and N. F. Ness, Saturn's ring current and inner magnetosphere, *Nature, 292,* 724, 1981.

Desch, M. D., and M. L. Kaiser, Voyager measurement of the rotation period of Saturn's magnetic field, *Geophys. Res. Lett., 8,* 253, 1981.

Goertz, C. K., M. F. Thomsen, and W.-H. Ip, Saturn's radio emissions: Rotational modulation, *Nature, 292,* 737, 1981.

Kaiser, M. L., M. D. Desch, and A. Lecacheux, Saturnian kilometric radiation: statistical properties and beam geometry, *Nature, 292,* 731, 1981.

Luhmann, J. G., and M. Schulz, Magnetic shell tracing: A simplified approach, in *Quantitative Modeling of Magnetospheric Processes, Geophys. Monogr. Ser.,* vol. 21, edited by W. P. Olsen, pp. 582–591, AGU, Washington, D. C., 1979.

Mead, G. D., Deformation of the Geomagnetic field by the solar wind, *J. Geophys. Res., 69,* 1181, 1964.

Ness, N. F., M. H. Acuña, R. P. Lepping, J. E. P. Connerney, K. W. Behannon, L. F. Burlaga, and F. M. Neubauer, Magnetic field studies by Voyager 1: Preliminary results at Saturn, *Science, 212,* 211, 1981.

Ness, N. F., M. H. Acuña, K. W. Behannon, L. F. Burlaga, J. E. P. Connerney, R. P. Lepping, and F. M. Neubauer, Magnetic field studies by Voyager 2: Preliminary results at Saturn, *Science, 215,* 558, 1982.

Powell, M. J. D., An efficient method for finding the minimum of a function of several variables without calculating derivatives, *Comput. J., 7,* 155, 1964.

Simpson, J. A., T. S. Bastian, D. L. Chenette, R. B. McKibben, and K. R. Pyle, The trapped radiations of Saturn and their absorption by satellites and rings, *J. Geophys. Res., 85,* 5731, 1980.

Smith, B. A., et al., Encounter with Saturn: Voyager 1 imaging science results, *Science, 212,* 163, 1981.

Smith, E. J., L. Davis, Jr., and D. E. Jones, Jupiter's magnetic field and magnetosphere, in *Jupiter,* edited by T. Gehrels, p. 788, The University of Arizona Press, Tucson, 1976.

Smith, E. J., L. Davis, Jr., D. E. Jones, P. J. Coleman, Jr., D. S. Colburn, P. Dyal, and C. P. Sonett, Saturn's magnetic field and magnetosphere, *Science, 207,* 407, 1980*a*.

Smith, E. J., L. Davis, Jr., D. E. Jones, P. J. Coleman, Jr., D. S. Colburn, P. Dyal, and C. P. Sonett, Saturn's magnetosphere and its interaction with the solar wind, *J. Geophys. Res., 85,* 5655, 1980*b*.

Smythe, W. R., *Static and Dynamic Electricity,* 3rd Edition, p. 295, McGraw-Hill, New York, 1968.

Van Allen, J. A., D. N. Baker, B. A. Randall, and D. D. Sentman, The magnetosphere of Jupiter as observed with Pioneer 10, 1, Instrument and principal findings, *J. Geophys. Res., 79,* 3559, 1974.

Vogt, R. E., D. L. Chenette, A. C. Cummings, T. L. Garrard, E. C. Stone, A. W. Schardt, J. H. Trainor, N. Lal, and F. B. McDonald, Energetic charged particles in Saturn's magnetosphere: Voyager 1 results, *Science, 212,* 231, 1981.

Vogt, R. E., D. L. Chenette, A. C. Cummings, T. L. Garrard, E. C. Stone, A. W. Schardt, J. H. Trainor, N. Lal, and F. B. McDonald, Energetic charged particles in Saturn's magnetosphere: Voyager 2 results, *Science, 215,* 577, 1982.

(Received February 22, 1982;
revised April 12, 1982;
accepted April 13, 1982.)